Int. J. Heat Mass Transfer. Vol. 28, No. 1, pp. 165–173, 1985
Printed in Great Britain

0017-9310/85 $3.00 + 0.00

Experimental study of natural convection in shallow enclosures with horizontal temperature and concentration gradients

Y. KAMOTANI, L. W. WANG, S. OSTRACH and H. D. JIANG
Department of Mechanical and Aerospace Engineering, Case Western Reserve University, Cleveland, OH 44106, U.S.A.

(*Received* 18 *January* 1984 *and in revised form* 22 *May* 1984)

Abstract—Natural convection in low aspect-ratio rectangular enclosures with combined horizontal temperature and concentration gradients is studied experimentally. An electrochemical system is employed to impose the concentration gradients. The solutal buoyancy force either opposes or augments the thermal buoyancy force. Due to a large difference between the thermal and solutal diffusion rates the flow possesses double-diffusive characteristics. Various complex flow patterns are observed with different experimental conditions. The temperature distributions and mass-transfer rates are also studied. A flow instability under certain conditions is reported.

1. INTRODUCTION

NATURAL convection in which the buoyant forces are due both to temperature and concentration gradients is generally referred to as thermosolutal convection or double-diffusive convection. As pointed out by Ostrach [1], various modes of convection are possible depending on how temperature and concentration gradients are oriented relative to each other as well as to gravity. Much attention has been given to the situation in which stratified fluids are subjected to imposed vertical temperature gradients in order to explain some unusual oceanographic phenomena (e.g. Turner [2]). For the same reason convection in stratified fluids with imposed horizontal temperature gradients has also been investigated (reviewed in [1]).

Thermosolutal convection is also important in crystal growth processes (Ostrach [3]). The transport process in the fluid phase during the growth of a crystal has a profound influence on the structure and quality of the solid phase. With the need for ever more perfect crystals, attention has begun to be focused on the role of convection in crystal growth. In many crystal growth techniques there are both temperature and concentration gradients in the fluid that can lead to buoyancy-driven convection. In some horizontal growth techniques (e.g. horizontal Bridgman) the fluid phase is subjected to horizontal temperature and concentration gradients. Several investigators in the past studied thermosolutal convection along a vertical flat plate (reviewed in [1]), but very little has been done on thermosolutal convection in an enclosure with combined horizontal temperature and concentration gradients, which motivated the present investigation. It is well known that thermal convection in an enclosure exhibits generally much more complex features than that along a vertical flat plate. Therefore, extensive experimental and theoretical work is needed to understand natural convection in an enclosure with combined driving forces. The present work is concerned with natural convection in a shallow rectangular enclosure with imposed horizontal temperature and concentration gradients (a typical configuration in horizontal crystal-growth methods). Its main objective is to obtain basic information on the resultant flows under various parametric conditions.

An electrochemical method based on a diffusion-controlled electrode reaction is employed in the present work for creating the concentration gradients. The horizontal temperature and concentration gradients are imposed in such a way that their effects on the flow are either opposing or augmenting. The flow structures and mass transfer rates are studied in detail under various conditions. The present paper is partially based on the work by Wang *et al.* [4].

2. EXPERIMENTAL DESIGN

2.1. *Dimensionless parameters*

Based on the basic differential equations for laminar, steady and two-dimensional natural convection in an enclosure with thermal and solutal buoyancy forces (see Fig. 1) it can be shown (Ostrach [1]) that the following dimensionless parameters are important in the problem.

$$Gr_T = \frac{g\beta\Delta T H^3}{\nu^2} \quad \text{thermal Grashof number}$$

$$Pr = \frac{\nu}{\alpha} \quad \text{Prandtl number}$$

$$Sc = \frac{\nu}{D} \quad \text{Schmidt number}$$

$$N = \frac{\bar{\beta}\Delta C}{\beta\Delta T} \quad \text{buoyancy ratio}$$

$$Ar = \frac{H}{L} \quad \text{aspect ratio}$$

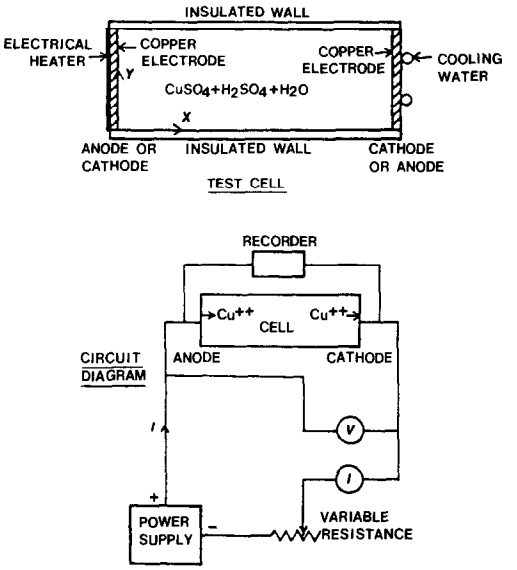

FIG. 1. Schematic of experimental system.

where g is the gravitational acceleration, v is the fluid kinematic viscosity, α the thermal diffusivity, and D the diffusion coefficient. The height and width of the enclosure are H and L, respectively. ΔT and ΔC are the imposed temperature and concentration differences, respectively, between the two vertical walls separated by L. Density variation due to temperature is represented by the volumetric thermal expansion coefficient β, and that due to concentration by the volumetric solutal expansion coefficient $\bar{\beta}$. Instead of the (Gr_T, N) combination the (Gr_T, Gr_S) combination is sometimes used, where Gr_s is defined as

$$Gr_s = \frac{g\bar{\beta}\Delta CH^3}{v^2} = N\,Gr_T \quad \text{solutal Grashof number.}$$

Among actual crystal systems the above parameters vary widely. For liquid metals Pr is about 0.01, and for aqueous solutions it is about 10. Sc is generally larger than Pr. For crystal growth using the horizontal Bridgman, open boat or closed-tube vapor deposition techniques, Ar is approximately in the range from 0.1 to 1. Gr_T is generally in the range from 10^4 to 10^6. Since it is impossible to cover such wide ranges of the parameters in the present experiment, and since the main object of the present study is to obtain basic information on natural convection due to the combined effects of temperature and concentration gradients in enclosures, the parametric ranges studied herein are mainly dictated by the electrochemical system employed herein to impose concentration gradients.

2.2. *Test apparatus*

A sketch of the present experimental system is given in Fig. 1. The figure also shows the coordinate system adopted herein. The test cell is a horizontally placed rectangular enclosure. Its width L is 7.6 cm, and the height H is variable to cover the range of Ar from 0.13 to 0.55. The depth of the enclosure is relatively large (25.4 cm) to obtain as close to two-dimensional flows as possible. The two vertical plates are made of 0.7 cm-thick copper plates and used as electrodes. An electrical heating mat is bonded to the back of one of the copper plates, and the other plate is cooled by circulating water from a constant-temperature bath. The other walls of the cell are made of 0.64 cm-thick plexiglas. The whole setup is enclosed by fiberglass insulation to mimimize the heat loss from the system to the surroundings. Some parts of the insulation can be removed to facilitate qualitative-flow structure observation. Three thermocouples are imbedded in each of the copper walls to determine the wall temperature.

A copper sulphate solution is used as electrolyte. When a voltage is applied to the electrodes, copper dissolves into the solution at the anode and is deposited at the cathode. As a result the density of the fluid near the cathode (anode) becomes lower (higher) than that of the bulk of the solution. The migration of the cupric ions in the electrical field is eliminated by adding sulphuric acid to the solution, which acts as a supporting electrolyte, and thus the transport of the cupric ions in the cell is controlled only by diffusion and convection. In the experiment the concentration of $CuSO_4$ varies from 0.05 to 0.08 M. The acidity of the solution is kept constant at 1.5 M H_2SO_4. The physical properties of the solution are taken from Wilke *et al.* [5].

The auxillary system consists of a d.c. power supply, instruments to measure the total current and potential in the cell, and a variable resistance to control the current.

With the present system the ranges of the dimensionless parameters covered are $Sc = 2100$, $Pr = 7$, $Gr_s = 1.4 \times 10^5$–1.0×10^7, $Gr_T = 0$–1.9×10^6 and $Ar = 0.13$–0.55. All the fluid properties are evaluated at the average temperature of the hot and cold walls, which is maintained at room temperature (21°C).

2.3. *Test procedure*

Although the temperatures of the copper walls can be easily measured by thermocouples, the concentration levels at the walls cannot be so easily determined. One relatively simple way to specify the concentration level at the cathode wall in the present system is to adjust the cell potential in such a way that the saturation current (limiting current) is obtained. Under the limiting-current condition the ion concentration at the cathode surface is zero, in other words the change in concentration across the solutal boundary layer along the cathode ((ΔC) cathode) is C_b, where C_b is the concentration level in the bulk fluid. The limiting-current condition is valid at the cathode but not along the anode surface. However, since the net mass fluxes at the cathode and anode are considered to be equal and since the concentration outside the solutal boundary layers of both walls is C_b, it is reasonable to expect that the average change in concentration across the solutal boundary layer along the anode ((ΔC) anode) is nearly

equal to (ΔC) cathode. Then the overall concentration difference across the cell is $\Delta C = (\Delta C)$ cathode + (ΔC) anode = $2C_b$, and thus Gr_s is defined based on $\Delta C = 2C_b$ in the present work. The above concept assumes that C_b remains constant, but as convection develops in the cell, the concentration level becomes non-uniform (stratified, as explained in the next section) in the bulk region, and only on the average the bulk concentration level remains constant. Moreover, due to electrolysis the copper wall surfaces become rough slowly with time, which means the current densities at the walls decrease and the condition at the cathode deviates gradually from the limiting-current condition. For this reason the duration of each run is limited to maximum 2–3 h, far shorter than the time required to attain steady solutal convection. All in all, the concentration boundary conditions at the walls are admittedly not as well-defined as the thermal conditions in the present work.

Three types of tests have been conducted. The first tests are done under isothermal conditions (pure solutal convection). In the second case the anode temperature is kept lower than the cathode temperature so that the thermal and solutal buoyancy forces cooperate (cooperating case). In the third case the anode temperature is higher than the cathode temperature (opposing case). In the last two cases the electrochemical system is started after the thermal convection becomes steady. If the system is started in other ways (e.g. the electrochemical is started first and then a temperature gradient is imposed), the concentration boundary conditions become less well-defined, since the limiting current has been found to change significantly with time as thermal convection developes in the cell. Prior to the present work pure thermal convection in enclosures similar to the one used herein have been investigated, and the results are reported in Kamotani *et al.* [6].

Flow patterns are studied by flow visualization. Since the color of the solution changes with cupric ion concentration, observing the color distribution gives us a good idea of flow configuration. To visualize local flow structures, dye streaks and small particles are also employed.

The temperature fields are investigated by a traversing thermocouple probe which is inserted into the enclosure through a narrow slit in the top wall.

3. RESULTS AND DISCUSSION

3.1. *Flow structure*

In the present electrochemical system operated under isothermal conditions the deposition of cupric ions on the cathode wall leaves behind less dense fluid. The lighter fluid rises to the top of the test section in a boundary-layer-type flow, and moves horizontally along the top wall. The downward flow in the boundary layer near the anode feeds heavier fluid along the bottom wall. The flow is confined to narrow regions along the vertical and horizontal walls, and the fluid in the balk (or core) region is stagnant. The fluid color changes gradually from the bottom to the top of the cell, indicating density stratification in the core.

It may be useful to compare in detail the above flow structure with that for purely thermal convection, because the overall flow structures look similar in both cases. If the enclosure dimensions are the same in both cases, the ratio of the thermal boundary-layer thickness along the vertical walls to the solutal boundary-layer thickness for Pr, $Sc > 1$ is given by (Wang *et al.* [4])

$$\frac{\delta_T}{\delta_S} = \left[\frac{Sc}{Pr} N\right]^{1/4}$$

In the present experiment $Pr = 7$ and $Sc = 2100$ and the buoyancy ratio parameter N is in the range between 4 and 40 typically so that δ_T/δ_S is larger than about 6. In fact δ_S is so small in the experiment (estimated to be on the order of 0.1 mm) that it is very difficult to observe visually the solutal boundary layers along the vertical walls. The ratio of the typical velocity in the thermal boundary layer to that in the solutal boundary layer is expressed as ([4])

$$\frac{V_T}{V_S} = \left(\frac{Sc}{Pr}\frac{1}{N}\right)^{1/2}.$$

The ratio is larger than 2.7 in the present experiment so that the solutal convection is generally slower than the thermal convection.

In the cooperating cases it could be anticipated that the flow structures are somewhat similar to those in purely thermal or solutal cases, i.e. unicellular flows. However, they are found to be more complex. Under certain conditions a layered flow pattern appears. A sketch of a typical layered flow-pattern observed with dye tracers for a cooperating case is given in Fig. 2. It can be seen that the fluid is layered into three cells with the sense of circulation in each layer being toward the anode (cold wall) along the top of each layer. The cell boundaries are clearly recognizable because the fluid

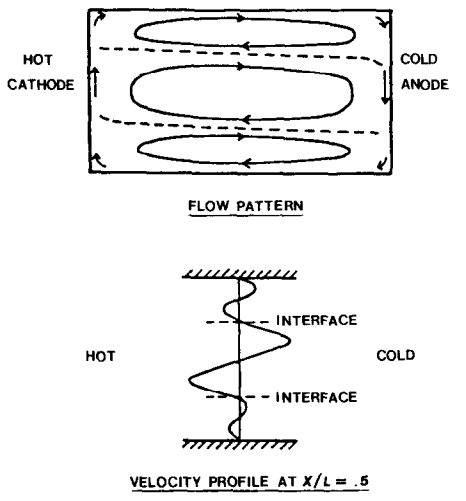

FIG. 2. Layered flow structure for cooperating case.

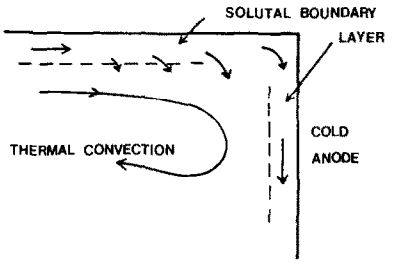

FIG. 3. Illustration of flow turning near cold anode leading to formation of top layer.

color changes sharply across them and is very uniform within each layer. Figure 2 also shows a typical dye streak distortion around $x/L = 0.5$. Generally the middle layer is the largest so that the velocity is larger there than those in the top and bottom layers. The velocity in the top (warm) layer is larger than that in the bottom (cold) layer mainly because of the fact that the viscosity of the fluid increases with decreasing temperature. The flow direction changes smoothly across each boundary without causing a shear instability in the ranges of the parameters studied herein. Such a layered flow structure is caused by the way the flow develops after the initiation of the electrochemical system. The following explanation is based on very careful flow observations. The lighter fluid in the solutal boundary layer moves up along the cathode wall and then flows along the top horizontal wall towards the anode. As illustrated in Fig. 3, when the fluid which is outside the solutal boundary layer and driven by the thermal gradient turns near the anode, it convects some of the lighter fluid into the region outside the solutal boundary layer along the anode wall. If the thermal driving face is relatively weak, the fluid in such mixed region becomes too light to be brought down along the anode by heat transfer and thus is pushed back towards the cathode, resulting in a cellular motion of the light fluid along the top wall. In the flow observation the top layer becomes visible near the cathode almost as soon as the electrochemical system is started and advances towards the anode where the light fluid is turned back. The same process described for the lighter fluid is applicable also to the heavier fluid along the bottom wall. The top and bottom layers become thicker with time as the lighter and heavier fluids accumulate in the respective regions, as seen in Fig. 4 which shows the change of layer thicknesses with time measured at $x/L = 0.5$ (mid-section). The time is measured from the time the limiting current is obtained. It takes about 30–45 min to reach the limiting current condition after starting the electrochemical system.

In Fig. 4 the temperature distributions measured at the mid-section are presented. As the layers develop, the initial profile due to pure thermal convection becomes quite distorted. In the main core region outside the top and bottom layers the temperature gradient becomes larger than that of the initial profile, which indicates

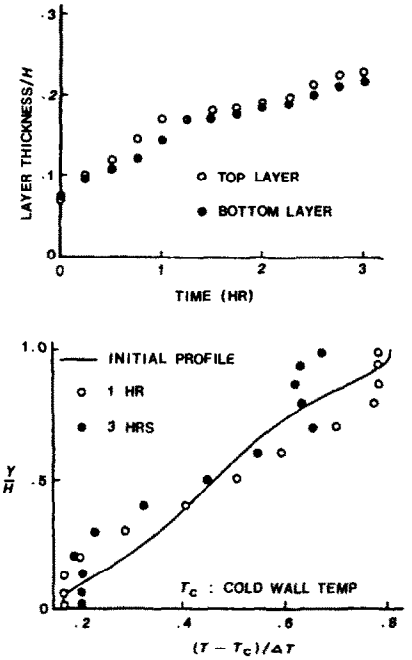

FIG. 4. Changes of layer thicknesses and temperature profile at mid-section for cooperating case with $Ar = 0.55$, $Gr_s = 1.0 \times 10^7$, $Gr_T = 5.4 \times 10^5$ and $N = 18.5$.

increased convection in the region as a result of cooperating body forces. The temperature distribution in each layer is determined by conduction across the layer and convection in the horizontal direction. When the layers are thin, the conduction dominates, and the temperature in each layer tends to be uniform across and equal to the temperature of the boundary with the

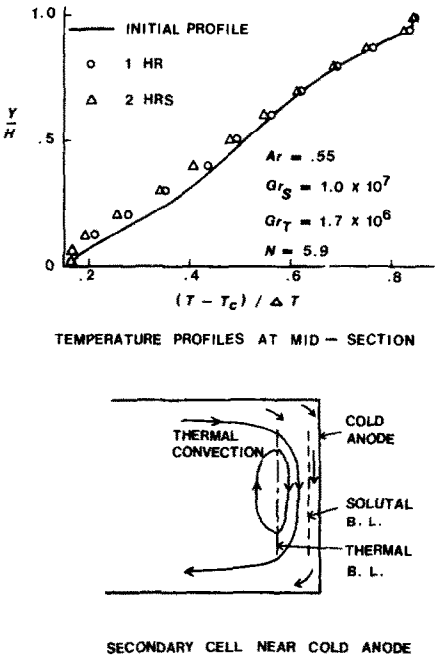

FIG. 5. Flow field for cooperating case with $N < 6$.

main core region. When the layers become thick, the convection becomes important, and the temperature level of the top (bottom) layer decreases (increases) because the convection within each layer is weaker than that in the main core region. The latter trend is not yet visible in Fig. 4 for the bottom layer because of slower convection caused by higher viscosity in the layer as explained above.

For fixed Gr_s and Ar if Gr_T is increased (or N is decreased), the layered flow pattern eventually disappears, because thermal convection becomes strong enough to bring down (up) the fluid near the anode (cathode). In the range of Ar studied herein the layers are found to disappear about $N = 6$. As shown in Fig. 5, when thermal convection becomes dominant, the temperature profiles at the mid-section are not influenced appreciably by the addition of solutal convection. However, near each vertical wall a secondary cell appears, as illustrated in Fig. 5. In the cell near the cold anode the flow is clockwise. The reason for the cell formation is considered to be as follows. Consider the region near the cold anode. Due to strong thermal convection less-concentrated fluid in the thermal boundary layer is brought down along the anode (the reason for the disappearance of the layered flow), but after the fluid turns around the bottom of the anode and moves out of the thermal boundary layer, the temperature increases while the concentration level is nearly constant, due to the fact the thermal diffusion process is much faster than the solutal diffusion process in the present experiment (the so-called double-diffusive phenomenon). As a result the flow acquires upward buoyancy after the turning and a secondary cell forms. It is noted that the cells do not exist in the initial thermal convection and appear only after the addition of solutal convection.

It is interesting that flow structures similar to those described above are observed even when the two body forces are opposed. For given Ar and Gr_s if Gr_T is small

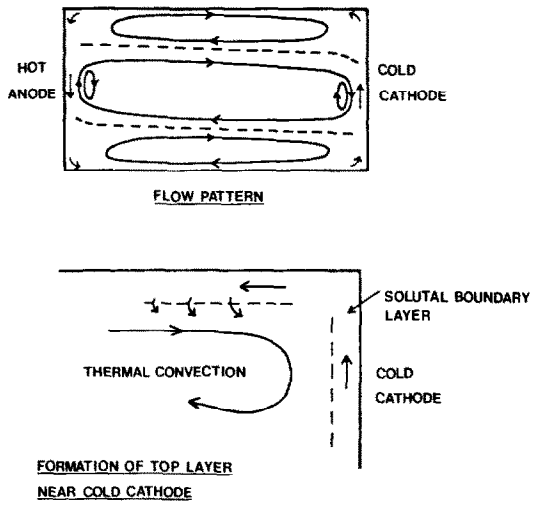

FIG. 6. Layered flow structure for opposing case.

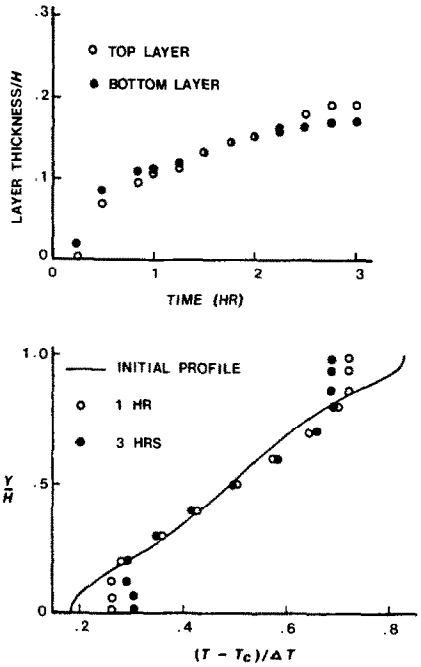

FIG. 7. Changes of layer thicknesses and temperature profile at mid-section for opposing case with $Ar = 0.55$, $Gr_s = 1.0 \times 10^7$, $Gr_T = 6.2 \times 10^5$ and $N = 16.2$.

enough, the layered flow structure appears also in the opposing case (Fig. 6). The reason for this is similar to that in the cooperating case, that is, less (more) concentrated fluid gets into thermal convection outside the solutal boundary layer and, as a result, it cannot be brought down (up) along the cold (hot) wall. But the mechanism of the mixing in the opposing case is a counter-flow mixing as illustrated in Fig. 6. The temperature profiles and the layer thicknesses measured at the mid-section are presented in Fig. 7. As in the cooperating case the layer thicknesses increase with time, but the initial temperature profile due to thermal convection does not change appreciably in the middle layer after the addition of solutal convection, which indicates less change in the thermal convection strength in the opposing case than in the corresponding (same Gr_T) cooperating case. The changes of temperature in the top and bottom layers follow similar trends to those in the cooperating case. Since in the opposing case the advancement of the top and bottom layers towards the center region after they are created is opposed by thermal convection, the layer thicknesses measured at the center are smaller than those for the cooperating case at the same time.

As in the cooperating case when N is decreased in the opposing situation, the layered flow-structure disappears. In the range of Ar studied herein it has been found to disappear if N is less than about 10. Near the condition where the layered flow disappears the flow directions in the solutal boundary layers along the vertical plates change. Due to strong shear exerted by the flow in the thermal boundary layer along, for example, the hot anode the fluid in the solutal boundary

layer is carried upward against the buoyancy force which acts downward in the solutal boundary layer if $N > 1$. However, when the flow turns near the top of the hot anode, the thermal convection slows down and the shear force associated with it decreases. Consequently, some of the heavy fluid goes down, resulting in a secondary cell near the anode. The same is true for the flow near the cold wall. Therefore, the flow structure for $N < 10$ in the opposing case is very similar to that in the cooperating case depicted in Fig. 5, but the reasons for the appearance of the secondary cells are different in both cases. If Ar, Gr_s and Gr_T are the same in both cases, the secondary cells in the opposing case appear to be stronger than those in the cooperating case, and in the former the fluid moves up and down nearly vertically so that the cells look flatter than the latter. Actually the mechanism described above works even when only some of the fluid in the solutal boundary layer is sheared against the buoyancy forces, that is, even when $N > 10$, and, as a result, weak secondary cells are seen in the middle layer of the layered flow-structure, as shown in Fig. 6. The temperature distributions measured at the mid-section are found to be not appreciably influenced by the addition of solutal convection, which means the overall heat transfer is not influenced very much by the complex flow structure near the vertical walls, but, as discussed later, the mass transfer is found to be substantially altered.

In both opposing and cooperating cases the layers appear when N becomes large enough. The layers are most clearly visible when N is between 15 and 30, but if N is increased further, their boundaries look increasingly diffused and the layer structure becomes less clear. It is noteworthy that in some trial runs both thermal and solutal driving forces were started at the same time, and the flow structures were found to be nearly identical to those discussed above with the same parametric ranges. Also in some cases solutal convection was started first, run long enough to establish a stable stratification in the core, and then thermal convection was added, under which condition several layered cells were observed to develop from the vertical walls and advance into the core region, the flow structure that has been studied in the past by Thorpe *et al.* [7] and Wirtz *et al.* [8].

3.2. *Mass transfer rate*

The mass transfer rate is determined under the limiting-current condition. With the limiting-current per unit area of the cathode (I_L) known the mass-transfer coefficient can be calculated as ([5])

$$h_c = \frac{I_L}{ZFC_b}$$

where F is Faraday's constant and Z is the charge number of reacting ion. The dimensionless mass transfer rate called Sherwood number is defined as

$$Sh = \frac{h_c H}{D}.$$

In the present electrochemical system the diffusion coefficient D is so small that it takes a long time to obtain truly steady solutal convection (H^2/D is on the order of several days), but the limiting current is measured within after the initiation of the electrochemical system. Thus, the mass transfer rate measured herein is not a steady-state value. However, the solutal boundary layer is considered to be established after the time scale δ_S^2/D which is on the order of 10 s, and at the end of the limiting-current measurement the aforementioned layers, if any, can be already seen. Therefore, the measured mass transfer rate is not expected to be much different from the steady-state value, and such accuracy may be sufficient in the present experiment in view of the aforementioned uncertainty in the concentration boundary conditions at the walls. The experimental error in the value of Sh is estimated to be $\pm 10\%$.

For pure thermal convection in low-aspect ratio enclosures it is known that when the parameter $Pr\ Gr_T$ becomes sufficiently large, the heat-transfer rate approaches to that of the corresponding vertical flat plate (Kamotani *et al.* [6]). A similar trend is anticipated also for mass-transfer rate. For this reason the past work on mass transfer in the combined thermal and solutal convection along a vertical flat plate is briefly discussed below.

In the previous flat plate work the combined Grashof number $GR = Gr_s + (Sc/Pr)^{1/2} Gr_T$ has been used sometimes. The parameter was originally obtained by Somers [9] in his integral analysis of the problem under the condition Pr, $Sc \sim 1$. Dan Bouter *et al.* [10] measured mass transfer rates using the same electrochemical system as the present one ($Pr \sim 7$, $Sc \sim 2100$), and correlated their data by the expression

$$Sh = c(Sc\ GR)^n \qquad (1)$$

with $n = 0.24$ and $c = 0.79$. They noted that the data scattered more in the opposing case than in the cooperating case. The above expression is based on the mass-transfer rate correlation for pure solutal convection ($GR = Gr_s$) along vertical plates. Wilke *et al.* [5] obtained $n = 0.25$ and $c = 0.68$ for that case in the same electrochemical system as the present one. Gebhart and Pera [11] made a numerical analysis of the combined convection along a vertical plate, and showed that for $Pr = 7$ and in the cooperating case Sh calculated by the integral method of Somers [9] is close to the numerical result up to $Sc = 500$ (maximum Sc computed), although the difference is appreciable for $Pr = 0.7$.

The mass transfer rates measured in the present experiment at fixed Ar and Gr_s and various Gr_T are given in Fig. 8 to show the effect of thermal convection on the mass transfer. In this section Gr_T is considered to be positive for the cooperating case and negative for the opposing case as in the definition of the parameter GR. As seen in Fig. 8, Sh becomes minimum at a certain negative value of Gr_T, which apparently corresponds to the situation where the effect of thermal convection on

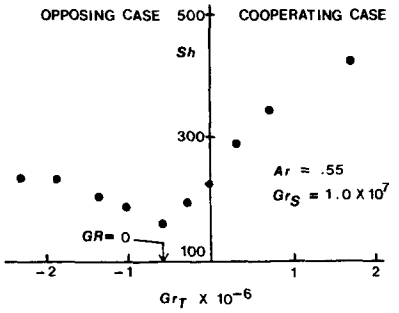

FIG. 8. Effect of thermal convection on mass transfer rate.

the mass transfer and that of solutal convection roughly cancel each other. According to equation (1) the situation occurs at $GR = 0$, and this point indeed lies around the point where Sh becomes minimum (but not zero as suggested by equation (1)) as seen in Fig. 8. If equation (1) is applicable to the present situation, Sh should be symmetric around $GR = 0$, but that is not the case, as apparent in Fig. 8. Sh does not increase with $|GR|$ in the negative GR region as much as it does in the positive GR region. In fact Sh is relatively constant in the negative GR region. The reason for this can be found from the above flow structure study. Thermal convection cannot really dominate the flow in the solutal boundary layer unless $|N| \ll 1$, while in the present experiment $|N| > 3$. Therefore, the flow in the solutal boundary layer is either slower than that in the isothermal case for large $|N|$ (N larger than about 10) or slowed down by the buoyancy force when it moves in the direction of thermal convection for smaller $|N|$. In the positive GR region (mostly in the cooperating region) Sh is a relatively strong function of Gr_T. Although the secondary cells appear also in the cooperating case if N is small enough, their effect on Sh is apparently overwhelmed by the increased level of convection due to cooperating body forces. In this regard the data for the cooperating case may be compared with those for vertical flat plates, because no secondary cell exists in the latter. In Fig. 9 the values of Sh measured under various conditions are plotted against the product $ScGR$. The data are compared with equation (1) with $n = 0.25$ and $C = 0.67$. The present data follow very closely the correlation curve for vertical flat plates. As mentioned earlier, the same trend has been observed for pure thermal convection in low aspect-ratio enclosures with sufficiently large $Pr\ Gr_T$ (larger than about 10^8). It is noted that the curve with $n = 0.24$ and $C = 0.79$ obtained by Dan Bouter *et al.* [10] follows very closely the curve in Fig. 9 in the present range of $ScGR$. Although one needs to be cautious because the present data are in a limited range of $ScGR$ and because of the aforementioned uncertainties in Sh and Gr_s, it seems that the mass transfer rate for the combined convection with cooperating body forces is close to that for the corresponding vertical flat plate as long as the parameter $ScGR$ is sufficiently large.

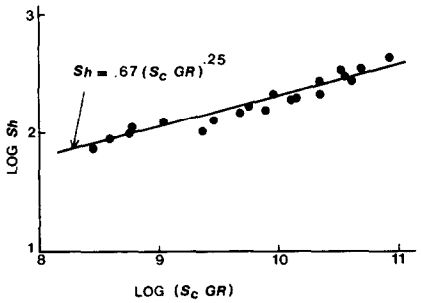

FIG. 9. Correlation of Sh for cooperating case.

3.3. *Flow instability*

Due to the aforementioned complex flow structure in the opposing case one might expect some kind of flow instability under certain conditions. That turns out to be the case. Shown in Fig. 10 are some examples of the cell potential variation with time. The cell potential variation is considered to be closely associated with the flow structure change in the solutal boundary layer. At $Ar = 0.13$ and $N = -17.4$ (opposing case) the call potential oscillates very sinusoidally with about a 40-s period. No such oscillation is found in the corresponding cooperating case with $N = 17.0$. The reason for the oscillation seems to be related to the mechanism for producing the secondary cells in the opposing case. As mentioned above, the secondary cells are created by the shear force associated with the flow in the thermal boundary layer. Consider the region near

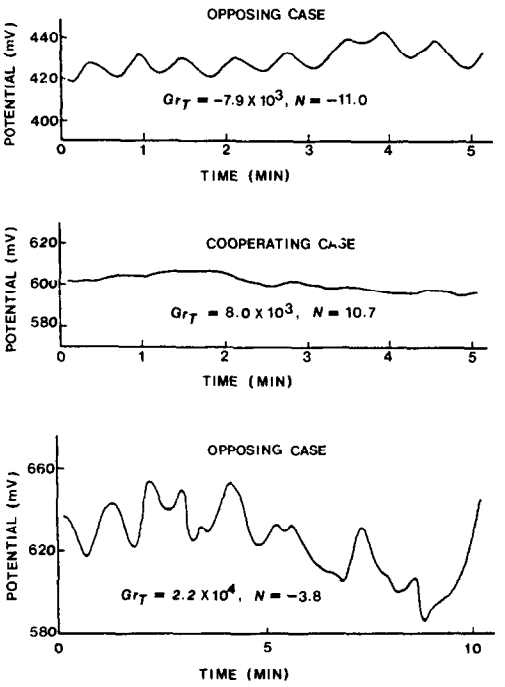

FIG. 10. Cell potential variations with time for $Ar = 0.13$ and $Gr_s = 8.6 \times 10^4$.

the hot anode. When the secondary cell forms, the downward motion in the secondary cell opposes the upward thermal convection, which may slow down the thermal convection to some extent and the shear may decrease. If that happens, the secondary cell weakens, the thermal convection revives, and the whole cyclic process starts again. In the cooperating case the secondary cells do not seem to be strong enough to cause such oscillation. If $|N|$ becomes large in the opposing case, the potential fluctuates rather randomly as seen in Fig. 10.

Since such unsteady characters of the flow have important implications for crystal growth processes, they will be studied in more detail in a separate paper.

4. SUMMARY

The purpose of the present experimental study is to investigate the effects of imposing horizontal concentration gradients on steady thermal convection in low aspect-ratio enclosures. The temperature and concentration gradients are imposed in such a way that their effects on the flow are either opposing and cooperating. The ranges of the parameters studied herein are $Sc = 2100$, $Pr = 7$, $Gr_T = 0$–1.9×10^6, $Gr_s = 1.4 \times 10^5$–1.0×10^7, $N \geqslant 3.8$ and $Ar = 0.13$–0.55. Under the present experimental conditions the solutal boundary layers along the vertical walls are much thinner than the thermal boundary layers. Due to double-diffusive phenomena various flow patterns appear in the enclosures depending on the ranges of the parameters.

In the cooperating case if N is larger than about 6, a three-layer structure appears. Within each layer the flow direction is determined by thermal convection. The top and bottom layers grow with time. If N is less than 6, the flow has a unicellular pattern with secondary cells near the vertical walls. Within the present parametric ranges and experimental errors, it seems that the mass transfer rate is close to that for the corresponding vertical flat plate.

In the opposing case if N is more than about 10, the flow is three-layered with secondary cells in the middle layer, and if N is smaller than 10, the flow is unicellular with secondary cells. The mass transfer rate does not change significantly with N. Under certain conditions the flow in the solutal boundary layer oscillates or fluctuates randomly.

Most of the results presented herein are somewhat qualitative, but they are believed to have general significance on crystal growth in an enclosure with horizontal concentration and temperature gradients.

REFERENCES

1. S. Ostrach, Natural convection with combined driving forces, *Physico Chem. Hydrodyn.* **1,** 233–247 (1980).
2. J. S. Turner, Double-diffusive phenomena, *Ann. Rev. Fluid Mech.* **6,** 37–56 (1974).
3. S. Ostrach, Fluid mechanics in crystal growth—the 1982 Freeman Scholar lecture, *J. Fluids Engng* **105,** 5–20 (1983).
4. L. W. Wang, Y. Kamotani and S. Ostrach, Experimental study of natural convection in a shallow horizontal cavity with different end temperatures and concentrations, Report FTAS/TR-82-164, Case Western Reserve University (1982).
5. C. R. Wilke, M. Eisenberg and C. W. Tobias, Correlation of limiting currents under free convection conditions, *J. Electrochem. Soc.* **100,** 513–523 (1953).
6. Y. Kamotani, L. W. Wang and S. Ostrach, Experiments on natural convection heat transfer in low aspect ratio enclosures, *AIAA J.* **21,** 290–294 (1983).
7. S. A. Thorpe, P. K. Hutt and R. Soulsby, The effect of horizontal gradients on thermohaline convection. *J. Fluid Mech.* **38,** 375–400 (1969).
8. R. A. Wirtz, C. F. Chen and D. B. Briggs, Stability of thermal convection in a salinity gradient due to lateral heating, *Int. J. Heat Mass Transfer* **14,** 57–66 (1971).
9. E. V. Somers, Theoretical considerations of combined thermal and mass transfer from a vertical flat plate, *J. appl. Mech.* **23,** 295–301 (1956).
10. J. A. De Leeuw Den Bouter, B. De Munnik and P. M. Heertzes, Simultaneous heat and mass transfer in laminar free convection from a vertical plate, *Chem. Eng. Sci.* **23,** 1185–1190 (1968).
11. B. Gebhart and L. Pera, The nature of vertical natural convection flows resulting from the combined buoyancy effects of thermal and mass diffusion, *Int. J. Heat Mass Transfer* **14,** 2025–2050 (1971).

ETUDE EXPERIMENTALE DE LA CONVECTION NATURELLE DANS DES ENCEINTES ETROITES AVEC DES GRADIENTS DE TEMPERATURE ET DE CONCENTRATION HORIZONTAUX

Résumé—On étudie expérimentalement la convection naturelle dans des enceintes rectangulaires à faible rapport de forme et avec des gradients combinés horizontaux de température et de concentration. Um système électrochimique est employé pour imposer les gradients de concentration. Les forces solutales de gravité s'opposent où favorisent les forces thermiques de gravité. A cause d'une grande différence entre les flux de diffusion thermique et massique l'écoulement possède des caractéristiques de double diffusion. Des configurations d'écoulement complexes et variées sont observées avec des conditions expérimentales différentes. On étudie les distributions de température et les flux de transfert massiques. On rapporte des conditions d'instabilité.

EXPERIMENTELLE UNTERSUCHUNG DER NATÜRLICHEN KONVEKTION IN FLACHEN HOHLRÄUMEN MIT HORIZONTALEN TEMPERATUR- UND KONZENTRATIONSGRADIENTEN

Zusammenfassung—Die natürliche Konvektion in rechteckigen Hohlräumen mit kleinem Höhen-Seitenverhältnis und horizontalen Temperatur- und Konzentrationsgradienten wird experimentell untersucht. Ein elektrochemisches System dient zur Erzeugung der Konzentrationsgradienten. Die Auftriebskraft infolge von Konzentrationsunterschieden wirkt gleich-oder gegensinnig zu derjenigen infolge von Temperaturdifferenzen. Wegen des großen Unterschieds zwischen der thermischen und der Konzentrations-Transportrate besitzt die Strömung Transporteigenschaften im doppelten Sinne. Unterschiedliche komplexe Strömungsmuster wurden unter verschiedenen Versuchsbedingungen beobachtet. Die Temperaturverteilungen und die Massentransportraten wurden ebenfalls untersucht. Über eine Strömungsinstabilität unter bestimmten Bedingungen wird berichtet.

ЭКСПЕРИМЕНТАЛЬНОЕ ИССЛЕДОВАНИЕ ЕСТЕСТВЕННОЙ КОНВЕКЦИИ В УЗКИХ ПОЛОСТЯХ С ГОРИЗОНТАЛЬНЫМИ ГРАДИЕНТАМИ ТЕМПЕРАТУРЫ И КОНЦЕНТРАЦИИ

Аннотация—Экспериментально изучена естественная конвекция в прямоугольных полостях с малым отношением сторон и комбинированными горизонтальными градиентами температуры и концентрации. Для задания градиента концентрации применялась электрохимическая система. Подъемная сила из-за переменной концентрации либо уменьшает, либо увеличивает термическую подъемную силу. Из-за большой разницы между скоростями термодиффузии и диффузии растворенного вещества течение имеет двойные диффузионные характеристики. Наблюдались различные сложные структуры течения при различных условиях эксперимента. Изучались также распределение температуры и коэффициенты массопереноса. Описана потеря устойчивости течения при определенных условиях.